Journal of
**Bioinformatics and Comparative Genomics**

JScholar
Fostering Scholarly Communication

Research Article Open Access

# Integrative Transcriptomics Reveals BDNF Hub Gene and FDA-Approved Drug Candidates for Diabetic Nephropathy

**Hafiz Rameez Khalid[1], Suhaira Hibba[2], Laiba Maqsood[3] and Sana Tabassum[4*]**

[1]International Joint Laboratory on Synthetic Biology and Biomass Biorefinery, Biofuels Institute, School of Emergency Management, School of the Environment and Safety Engineering, Jiangsu University, China
[2]School of Basic Medical Science, Chongqing Medical University, China
[3]Department of Bioinformatics & Biotechnology, Government College University Faisalabad (GCUF), Pakistan
[4]Center for Obesity and Metabolic Diseases Research, School of Basic Medical Science, Chongqing Medical University, China

[*]**Corresponding Author:** Sana Tabassum, Center for Obesity and Metabolic Diseases Research, School of Basic Medical Science, Chongqing Medical University, China.

**Received Date:** July 20, 2026 **Accepted Date:** August 08, 2026 **Published Date:** August 11, 2026

**Citation:** Hafiz Rameez Khalid, Suhaira Hibba, Laiba Maqsood, Sana Tabassum (2026) Integrative Transcriptomics Reveals BDNF Hub Gene and FDA-Approved Drug Candidates for Diabetic Nephropathy. J Bioinfo Comp Genom 7: 1-15

## Abstract

**Objectives:** Diabetic Nephropathy is a major microvascular consequence of diabetes mellitus, which is considered to be one of the main causes of end-stage renal disease. However, the molecular mechanisms of DN progression are still poorly understood. In our study, we performed an RNA-seq analysis to compare the diseased and normal tissue samples.

**Study Design:** We analyzed the raw sequencing data using the SRA toolkit, followed by quality control, read alignment, and normalization. We performed differential expression, functional enrichment, miRNA-hub gene interaction, and weighted gene co-expression network analysis. We chose Brain-Derived Neurotrophic Factor for structure-based screening, followed by virtual screening of FDA-approved drugs, molecular docking, and MD simulations. Functional enrichment indicated that mitochondrial dysfunction, oxidative stress, and metabolic dysregulation had been involved in DN progression.

**Results:** We identified 147 up-regulated and 56 down-regulated genes. WGCNA and PPI analyses indicated that BDNF was a hub gene that was extensively regulated by miRNAs. Virtual screening and docking indicated that Glimepiride, Lidoflazine, and Paliperidone were high-affinity modulators of BDNF. MD simulations confirmed that these molecules were bound to BDNF and interacted with it persistently.

**Conclusion:** These findings provide a comprehensive molecular framework for DN and highlight BDNF-targeting FDA-approved drugs as promising candidates for therapeutic repurposing.

**Keywords**: RNA-sequencing, Diabetic nephropathy, DEGs, Molecular Docking, WGCNA, Brain-Derived Neurotrophic Factor

## Introduction

One of the most common and severe complications of diabetes mellitus is diabetic nephropathy [1]. It is associated with a high mortality and morbidity rate among diabetic patients [2]. Diabetic nephropathy's etiology and its recurrence are a complex and multifactorial process [3]. A number of factors and regulators are involved in this process [4]. Alteration in hemodynamic and metabolic factors triggers a number of transcription factors and signal transduction pathways [5]. This process leads to the production of inflammatory mediators and growth factors [6]. This process ultimately causes the buildup of cellular and extracellular proteins and proteinuria, resulting in altered vascular permeability and the development of diabetic nephropathy [7]. A number of researchers around the world have worked on the pathogenesis of diabetic nephropathy. The actual pathological process and molecular incidence of diabetic nephropathy are still unknown [8].

The RNA-seq technique has revolutionized the field of transcriptomics, as it has transformed the understanding of the size of the transcriptome [9]. RNA sequencing is an efficient technique for understanding the fundamental expression of genes, as it provides an even more accurate measure of expression patterns than other techniques, allowing researchers to identify transcripts based on minimum amounts [10]. The use of RNA-Seq (RNA sequencing) for the identification of fluctuations in gene expression levels has become widely recognized in the scientific community [11]. This method is more comprehensive than gene chips or other sequencing methods for mapping and identifying transcriptomes [12]. Even though RNA-Seq generates a huge amount of data, bioinformatics is capable of analyzing the data in a complete, comprehensive, and appropriate way. Consequently, this method aims to discover the genes linked with human disease [13] from the high-throughput data collected from it [14]. Due to advances in bioinformatics technology, the availability of many public databases, and the application of analytical methods, powerful tools for analyzing and distinguishing between differentially expressed genes have been developed [15]. If you relate this approach to other sequencing methods, it offers a complete way of mapping and quantifying transcriptomes [16]. The growing number of diverse public datasets and the adoption of analytical methods have provided strong resources for the study and discovery of genes that are expressed differently. Recently, integrated transcriptome analysis based on publicly available RNA-sequencing data has facilitated a robust discovery of disease-associated expression signatures with improved sample size and diminished study-specific bias. Network-based methods such as WGCNA have also contributed beyond traditional expression analysis to highlight biologically functional gene modules strongly linked to disease phenotype. In addition, the role of microRNAs (miRNAs), a class of gene expression regulators and transcripts at the post-transcriptional level, cannot be underestimated in the disease progression pathway of diabetic nephropathy. An integrated analysis of gene expression profiling, the role of microRNAs with their network regulation, and in silico drug repositioning can be a promising beginning for a new therapeutic targeting discovery platform [17].

In the proposed study, we performed an integrated transcriptomic analysis to explore the molecular mechanisms underlying diabetic nephropathy. High-throughput RNA-Seq data from publicly available datasets were retrieved, processed, and analyzed to identify differential expression of genes between diseased and healthy persons. To uncover biologically meaningful patterns, we constructed gene co-expression networks using WGCNA and PPI networks to identify key hub genes. The regulatory role of microRNAs (miRNAs) was further investigated by building

hub gene–miRNA interaction networks. Finally, one of the top hub genes, Brain-Derived Neurotrophic Factor (BDNF), was selected for structure-based analysis, where virtual screening, molecular docking, and molecular dynamics simulations were conducted to explore potential FDA-approved drugs for therapeutic repurposing. This integrative approach is designed to provide a systematic framework for understanding gene regulation in diabetic nephropathy and lay the groundwork for identifying potential molecular targets for future therapeutic intervention.

## Methodology

### Data Retrieval

The samples from humans of diabetic nephropathy used were obtained from the NCBI Gene Expression Omnibus (GEO) database. The selected datasets included 5 DN and 5 healthy control samples generated using Illumina HiSeq [18]. In addition to, four different studies (GSE154881, GSE142025, GSE17579, and GSE162830) were incorporated, containing a total of 45 control and 53 DN samples. All samples represented biological replicates and captured inherent biological variability. Raw sequencing data were downloaded using the SRA Toolkit (prefetch) and converted into FASTQ.gz format for downstream analysis [19].

### Preprocessing, Alignment and Annotation of Reads

Quality assessment of raw sequencing reads was performed using FastQC. Low-quality reads were filtered using Sickle with default parameters (quality cutoff = 1). Adapter sequences and residual low-quality bases were removed using Trim Galore and CutAdapt, which apply semi-global alignment to minimize sequence bias. The human reference genome, was obtained from the Ensembl genome browser in FASTA format. Genome indexing was performed using Bowtie2-build, and high-quality trimmed reads were aligned to the reference genome using Bowtie2-align. The resulting alignments were stored in BAM format. SAM tools were used to remove redundant reads to improve mapping reliability.

The genes present in each samples were quantified using high-throughput HTseq-count [20]. Htseq-count identified and counted reads through the de novo annotation feature, including those spanning multiple exons. Moreover, uses the GTF coordinate with the SAM alignment file to map the genome and assign reads. The counted data were displayed as a matrix, representing the number of sequence reads assigned to each gene across all samples.

### Differentially expressed genes (DEGs) profiling

DESeq2 package from Bioconductor was utilized to identify the DEGs from Bioconductor. Raw count data were organized into a tabular format, with genes as rows and samples as columns. The Pasilla package was used to validate HTSeq count consistency and experimental grouping. Normalization and variance estimation were performed using DESeq2's internal modeling. Variance stabilization was achieved using both variances stabilizing transformation (VST) and the regularized log (rlog) transformation. Genes with an adjusted p-value $< 0.05$ and $\log_2 FC \geq 1$ were considered as significant.

Functional annotation and pathway enrichment analyses were carried out using cluster Profiler, enrich plot, and DOSE packages. The Gene Ontology (GO) analysis was carried out for biological processes, molecular functions, and cellular components. In addition, the KEGG pathways analysis was used to identify important pathways that are affected. The top enriched GO terms and KEGG pathways were visualized using ggplot2, with a cutoff value of $p < 0.05$.

### Weighted Gene Co-expression Network Analysis (WGCNA)

Gene co-expression networks were built using the WGCNA package version 1.72-1 in R software. Genes with too many missing values were filtered out, and samples that were outliers were removed using hierarchical clustering. The soft-thresholding power $\beta$ was set at 7 using the pick Soft Threshold function to satisfy scale-free topology. An adjacency matrix was constructed and transformed into a topological overlap matrix (TOM) to assess network connectivity. Hierarchical clustering coupled with the dynamic tree cut approach was used to identify gene modules, with a minimum module size of 30 genes. Module eigengenes were calculated to depict module expression patterns. Module–trait

associations were evaluated using Pearson's correlation analysis, based on experimental conditions (DN vs. control). Statistically significant modules were subjected to enrichment analysis, and results were visualized using dot plots, ridge plots, and enrichment plots to identify key biological drivers.

### Construction of Hub Gene–miRNA Interaction Network

To identify the miRNAs targeted the hub genes, six ENCORI-supported databases including miRanda, miRmap, PITA, microT, PicTar, and Traget scan were analyzed. Using the Cystoscope software, a miRNA-target network was generated to visualize the interactions among the identified miRNAs and hub-genes. (Figure 4). miRNA detected in at least three of the six databases were considered reliable target miRNAs for the corresponding hub-genes [21,22].

### Virtual Screening and Molecular Docking Analysis

The three-dimensional structure of Brain-Derived Neurotrophic Factor (BDNF) was obtained from the Protein Data Bank (ID: 8OYD). Protein preparation subjected to energy minimize involved the removal of all water molecules and non-protein ions to obtain a receptor structure suitable for docking studies. Virtual screening was performed using the DrugRep server, targeting FDA-approved compounds to identify potential modulators of BDNF. The ten compounds were screened based on their binding affinity toward BDNF. Among them, the ranked top three compounds including Glimepiride, Lidoflazine, and Paliperidone were exhibiting the highest binding score affinity were selected for downstream analysis. Docking was performed using AutoDock Vina for the binding affinity and preferred binding orientations of the selected drugs within the BDNF binding pocket. Using UCSF Chimera for further visualized the protein complex.

### Molecular Dynamic Simulation

To evaluate the dynamic stability and conformational behavior of the docked protein–ligand complexes, all-atom molecular dynamics (MD) simulations were performed for a total duration of 200 ns[23]s. Based on docking scores and interaction profiles, the three highest-ranked FDA-approved compounds including Glimepiride, Lidoflazine, and Paliperidone were selected for MD validation in complex with the target protein. MD simulations were performed using the GROMACS simulation package under periodic boundary conditions. The protein topology was generated using the CHARMM36 force field, while ligand parameters were obtained from the CHARMM General Force Field (CGenFF). Each protein–ligand complex was solvated in a triclinic simulation box using the TIP3P water model, ensuring a minimum distance of 10 Å between the protein surface and the box boundaries. The systems were electrically neutralized using the appropriate Na+ and Cl- counter ions. Energy minimization of the systems was done using the steepest descent method, whereby the systems converged based on the maximum force, which had to be below 1000 kJ/mol/nm.

After minimization, the systems were then subjected to equilibration, whereby two different conditions were used. Initially, the NVT ensemble was used to maintain the temperature of the systems at 300 K, where the V-rescale method was employed. Subsequently, the NPT ensemble was used, maintaining the systems at 1 bar, where the Parrinello-Rahman barostat method was employed[24]. All bonds containing hydrogen atoms were limited by the LINCS algorithm, allowing for a 2 fs time step. Long-range electrostatic interactions were achieved using the Particle Mesh Ewald method, whereby the cutoff distance of 1.0 nm was employed for both Coulombic and van der Waals interactions. Post-simulation trajectory analyses were done using built-in facilities of GROMACS to assess the stability of the complexes. Parameters of interest included the root mean square deviation, root mean square fluctuation, solvent-accessible surface area, as well as hydrogen bond formation, all of which were done throughout the simulation period.

## Results

### Comprehensive Differential Gene Expression Analysis

To identify genes showing significant changes in expression between diabetic nephropathy (DN) and normal tissues, we carried out genome-wide differential expression

analysis of 98 samples, including 53 DN samples and 45 controls, across four independent GEO datasets. Our analysis revealed 203 significant DEGs, including 147 upregulated genes (72.4%) and 56 downregulated genes (27.6%) (log2FC > 1, adj p value < 0.05). This indicates the upregulated nature of the DEGs, as seen in the transcriptional profile of DN pathogenesis.

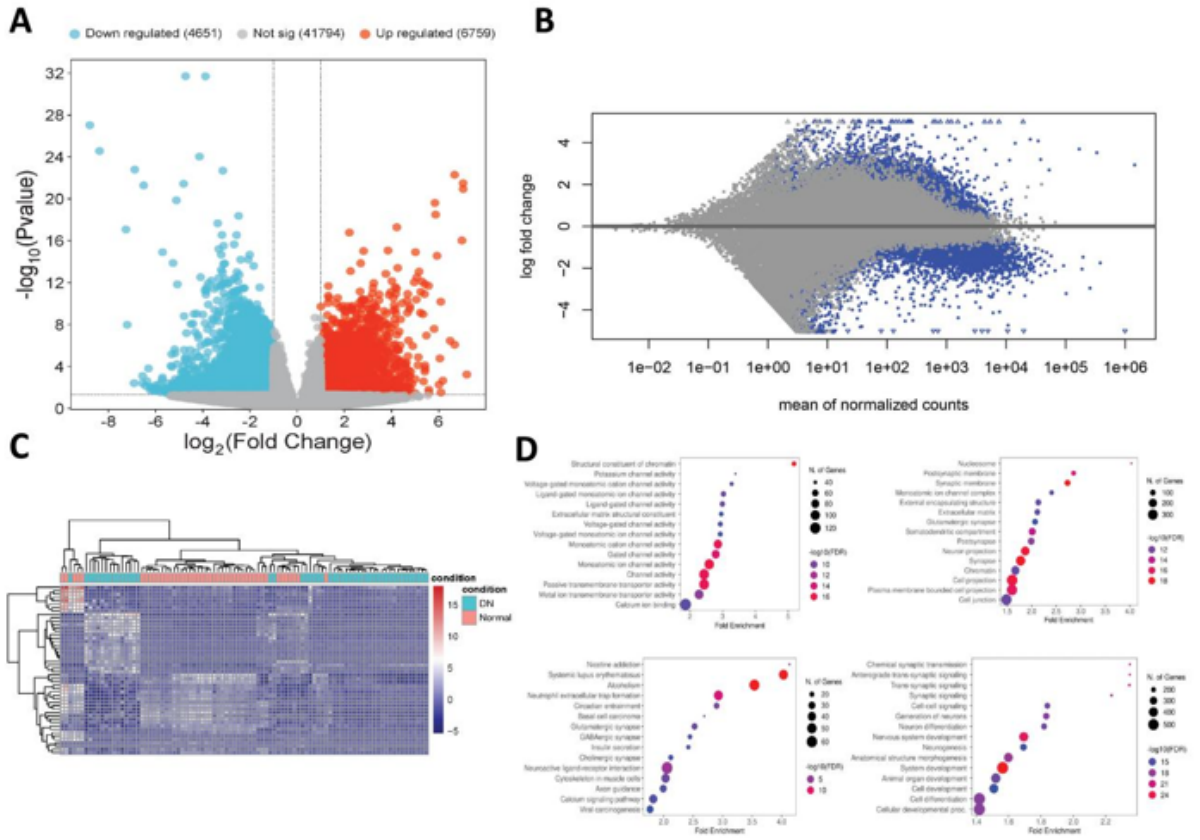


**Figure 1:** shows the landscape of differential gene expression in diabetic nephropathy.(A) A volcano plot showing the genes (DEGs) that are significantly different in diabetic nephropathy (DN) and control samples. Significantly downregulated genes (adjusted $p < 0.05$, $|\log_2 FC| \geq 1$) are indicated by blue dots, significantly upregulated genes by red dots, and non-significant genes by grey dots.(B) MA plot illustrating the correlation between $\log_2$ fold change and mean normalised counts. Genes that have undergone significant alteration and exhibit strong transcriptional divergence are highlighted. (C) A heatmap of the top DEGs using hierarchical clustering that clearly separates the DN and control samples. Rows represent genes, and columns show individual samples. These are grouped according to Euclidean distance and complete linkage. (D) Analysis of differentially expressed genes using functional enrichment. Gene Ontology (GO) molecular function enrichment reveals a notable overrepresentation of structural ribosomal components and oxidoreductase activity. GO cellular component analysis showing cytosolic ribosomal subunits and mitochondrial respiratory chain complexes. KEGG pathway enrichment analysis showing strong participation in carbon metabolism, reactive oxygen species (ROS) pathways, and oxidative phosphorylation.

## Pathway and Functional Enrichment Reveal Metabolic Dysregulation and Mitochondrial Dysfunction

In order to elucidate the biological significance of the identified DEGs, functional enrichment analysis was performed. Gene Ontology (GO) indicated that DEGs were significantly associated with oxidoreductase activity, electron transfer, and structural constituents of ribosomes, indicating the disruption of metabolic processes. Moreover, structural constituents of ribosomes were found to be highly enriched, indicating the disruption of protein synthesis machinery (Figure 1D). The most significant functional localization of DEGs was found to be mitochondrial respirato-

ry chain complexes and cytosolic ribosomal subunits, indicating that DN pathogenesis primarily involves the disruption of mitochondrial integrity and protein translation machinery (Figure 1D). Aerobic respiration, oxidative phosphorylation, and ATP synthesis-coupled electron transport were found to be substantially correlated with DEGs. This suggests that disrupted mitochondrial bioenergetics is a major hallmark of DN (Figure 1D). In addition, KEGG pathway enrichment analysis reinforced these findings by showing that the DEGs were mainly associated with pathways of oxidative phosphorylation, carbon metabolism, and ROS, which are specific pathways of metabolic stress and mitochondrial dysfunction that occur in the hyperglycemic kidney tissue. Overall, these enrichment analyses support that metabolic rewiring and mitochondrial oxidative stress are major mechanisms underlying kidney injury in diabetic nephropathy (Figure 1D).

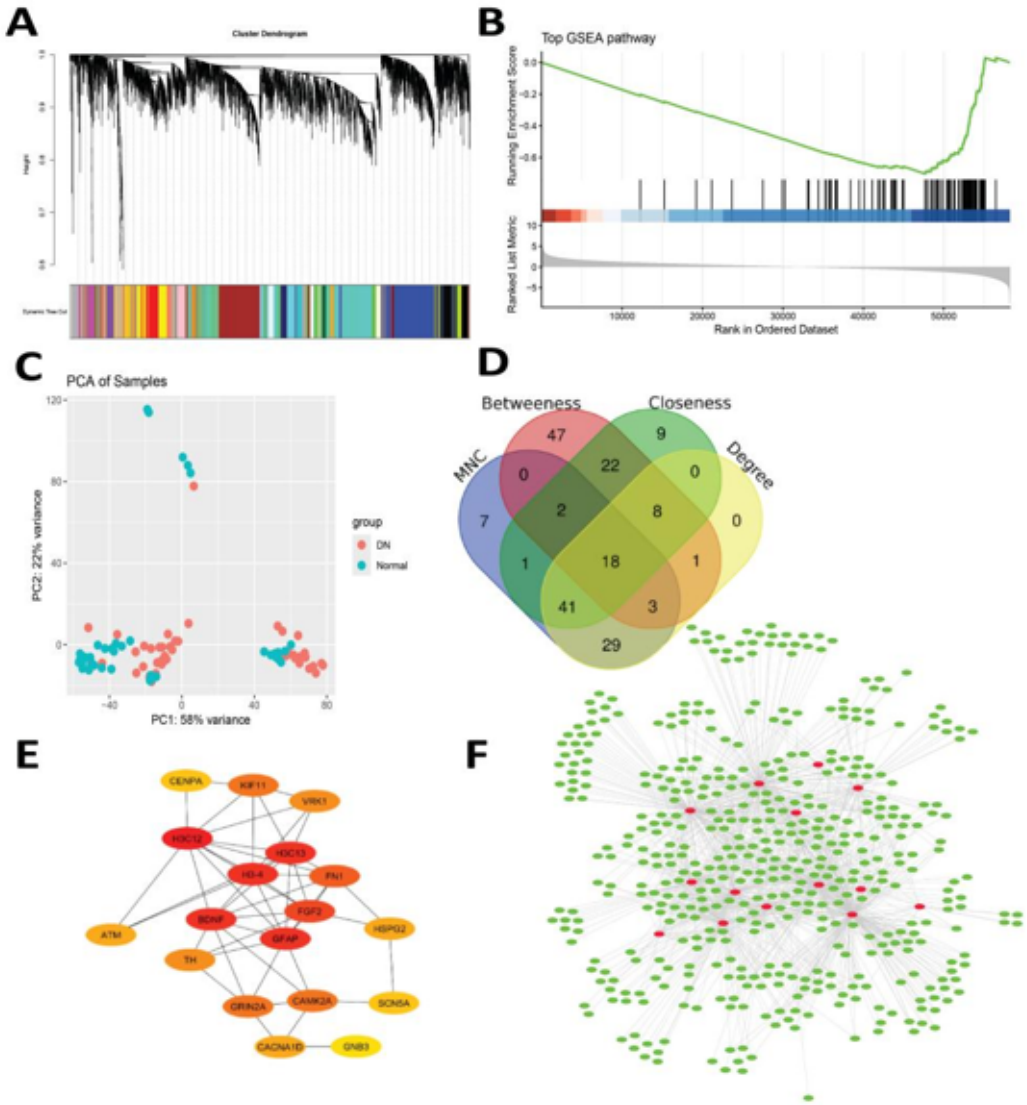


**Figure 2:** Global transcriptomic reprogramming and co-expression networks in DN. (A) Gene modules identified by Weighted Gene Co-expression Network Analysis (WGCNA) in a hierarchical clustering dendrogram. Clusters of highly co-expressed genes are represented by distinct modules, which are colour-coded. (B)DN samples exhibit positive enrichment of electron transport chain pathways and oxidative phosphorylation, according to Gene Set Enrichment Analysis (GSEA). (C) Global transcriptomic changes are indicated by a Principal Component Analysis (PCA) plot that clearly separates the DN and control samples. (D) Cytoscape visualisation of the STRING-derived PPI network built from significant DEGs. Proteins are represented by nodes, and functional interactions are represented by edges. (E) Using the degree, MNC, and betweenness centrality algorithms, cytoHubba is used to identify hub genes. The genes with the highest rankings—BDNF, ATM, GFAP, FGF2, and

FN1—are highlighted, signifying their crucial regulatory functions in the pathophysiology of DN. (F) shows the network of miRNA-hub gene regulatory interactions.Hub genes and the projected miRNAs that target them are visualised in a network using six ENCORI-supported datasets (miRanda, miRmap, PITA, microT, PicTar, and TargetScan). Hub genes (circles) and miRNAs (triangles) are represented by nodes, and putative regulatory connections backed by at least three databases are indicated by edges. Extensive miRNA interaction between BDNF and ATM indicates robust post-transcriptional regulation.

**Table 1:** Top-ranked genes identified from the STRING protein–protein interaction (PPI) network based on the Degree method.

| RankNo. | Name | Score | Gene Symbol |
|---|---|---|---|
| 1 | 9606.ENSP00000352252 | 10 | H3C12 |
| 2 | 9606.ENSP00000414303 | 9 | BDNF |
| 2 | 9606.ENSP00000355657 | 9 | H3-4 |
| 2 | 9606.ENSP00000333277 | 9 | H3C13 |
| 2 | 9606.ENSP00000253408 | 9 | GFAP |
| 6 | 9606.ENSP00000264498 | 8 | FGF2 |
| 7 | 9606.ENSP00000346839 | 7 | FN1 |
| 8 | 9606.ENSP00000260731 | 5 | KIF11 |
| 8 | 9606.ENSP00000332549 | 5 | GRIN2A |
| 8 | 9606.ENSP00000500386 | 5 | CAMK2A |
| 11 | 9606.ENSP00000370571 | 4 | TH |
| 11 | 9606.ENSP00000216639 | 4 | VRK1 |
| 13 | 9606.ENSP00000363827 | 3 | HSPG2 |
| 13 | 9606.ENSP00000278616 | 3 | ATM |
| 13 | 9606.ENSP00000288139 | 3 | CACNA1D |
| 16 | 9606.ENSP00000328968 | 2 | SCN5A |
| 16 | 9606.ENSP00000336868 | 2 | CENPA |
| 18 | 9606.ENSP00000229264 | 1 | GNB3 |

## Co-expression Network Analysis Identifies Metabolic Gene Modules

Weighted Gene Co-expression Network Analysis (WGCNA) has identified several modules of co-expressed genes involved in different biological processes in the context of DN. Hierarchical cluster analysis (Figure 2A) has identified sets of co-regulated genes that most likely participate in mitochondrial metabolism, oxidative stress, and inflammatory signaling pathways. PCA has also shown the separation between the two groups (Figure 2C), indicating that there is globally significant transcriptional reprogramming in the context of a characteristic molecular signature, including the presence of metabolic dysregulation and mitochondrial damage in the context of DN. GSEA result showed significant positive enrichment of the pathways involved in oxidative phosphorylation and electron transport chain activity in the DN tissue (Figure 2B). This may indicate a compensatory response to oxidative stress resulting from the effect of hyperglycemia. The result of the combination of WGCNA and GSEA analysis again points towards the central role of mitochondrial dysfunction in the pathoge-

nesis of diabetic nephropathy.

## Protein-Protein Interaction Network Identifies 18 Hub Genes

To identify core regulatory components of DN pathogenesis, we generated a protein-protein interaction (PPI) network of DEGs using STRING database server and analyzed it with Cytoscape's cytoHubba plugin. Three topological approaches (degree, MNC, and betweenness centrality) of our study identified 18 high-confidence hub genes (Figure 2D-E). These hub genes were found to display substantially increased connectivity, which is indicative of their importance in DN molecular architecture. Hub gene network revealed that key components of DN pathogenesis include H3C12, BDNF, GFAP, FGF2, FN1, etc., which are involved in various biological processes.

**Table 2:** Molecular docking results showing the binding energy and molecular weight (MW) of the selected drug compounds.

| DrugID | Name | Formula | Binding energy | MW |
|---|---|---|---|---|
| DB00696 | Ergotamine | $C_{33}H_{35}N_5O_5$ | -29.0 | 581.6615 |
| DB13766 | Lidoflazine | $C_{30}H_{35}F_2N_3O$ | -36.7 | 491.627 |
| DB01267 | Paliperidone | $C_{23}H_{27}FN_4O_3$ | -35.2 | 426.4839 |
| DB00222 | Glimepiride | $C_{24}H_{34}N_4O_5S$ | -35.0 | 490.62 |
| DB00941 | Hexafluronium | $C_{36}H_{42}N_2$ | -34.3 | 502.745 |
| DB00549 | Zafirlukast | $C_{31}H_{33}N_3O_6S$ | -34.2 | 575.675 |
| DB06210 | Eltrombopag | $C_{25}H_{22}N_4O_4$ | -34.0 | 442.4666 |
| DB00224 | Indinavir | $C_{36}H_{47}N_5O_4$ | -33.8 | 613.7895 |
| DB00490 | Buspirone | $C_{21}H_{31}N_5O_2$ | -32.6 | 385.5031 |
| DB00947 | Fulvestrant | $C_{32}H_{47}F_5O_3S$ | -32.5 | 606.78 |

## miRNA Regulatory Network and Hub Gene Prioritization

In order to comprehend the concept of post-transcriptional regulation, we built a miRNA hub gene interaction network using six data sources that were supported by the ENCORI tool, including miRanda, miRmap, PITA, microT, PicTar, and TargetScan. This led to the identification of 12 major hub genes that were targeted by multiple miRNAs, including BDNF, ATM, CACNA1D, CAMK2A, CENPA, FN1, FGF2, GFAP, GNB3, GRIN2A, H3C12, and VRK1) targeted by multiple miRNAs (Figure 2F), indicating their importance in DN regulatory networks.

Notably, ATM and BDNF demonstrated the strongest connectivity, each targeted by numerous miRNAs including hsa-miR-181b-5p, hsa-miR-211-5p, and hsa-miR-140-3p, positioning them as critical regulatory nodes. Similarly, CACNA1D and VRK1 experienced widespread miRNA regulation through hsa-miR-135a-5p, hsa-miR-374a-5p, and hsa-miR-17-5p. Based on network connectivity and hub gene identification, BDNF (Brain-Derived Neurotrophic Factor) emerged as the highest-ranked biomarker candidate, exhibiting both strong network centrality and extensive miRNA-mediated regulation.

## Virtual Screening and Molecular Docking Identifies FDA-Approved Drug Candidates

To identify therapeutic modulators of BDNF, we performed virtual screening of FDA-approved compounds against the BDNF structure (PDB ID: 8OYD) using the DrugRep server. The screening evaluated binding affinity for 5000+ FDA-approved drugs. The top 10 compounds were ranked by binding scores, with Glimepiride (ΔG = -35.0 kcal/mol), Lidoflazine (ΔG = -36.7 kcal/mol), and Paliperi-

done (ΔG = -35.2 kcal/mol) showing the highest predicted affinities. Detailed molecular docking analysis (Figure 3) using AutoDock Vina integrated within PyRx was performed for these three lead compounds. Ligand preparation involved 3D coordinate generation and energy minimization using OpenBabel, followed by PDBQT format conversion. The top-scoring docking conformations were visualized in Chimera to analyze interaction profiles.

The docking study was performed by employing **AutoDock Vina**, indicated that Glimepiride forms an extensive hydrogen bonding network with crucial BDNF residues, in addition to the formation of hydrophobic interactions within the binding pocket. Whereas, the highest binding affinity is found in Lidoflazine, where π-stacking interactions also help in the stabilization of the complex. Moreover, Paliperidone forms high electrostatic interactions, along with moderate hydrogen bonding, and is also found to have the potential to significantly stabilize the protein conformation. These structural predictions suggest promising therapeutic potential for repositioning these FDA-approved agents as DN modulators.

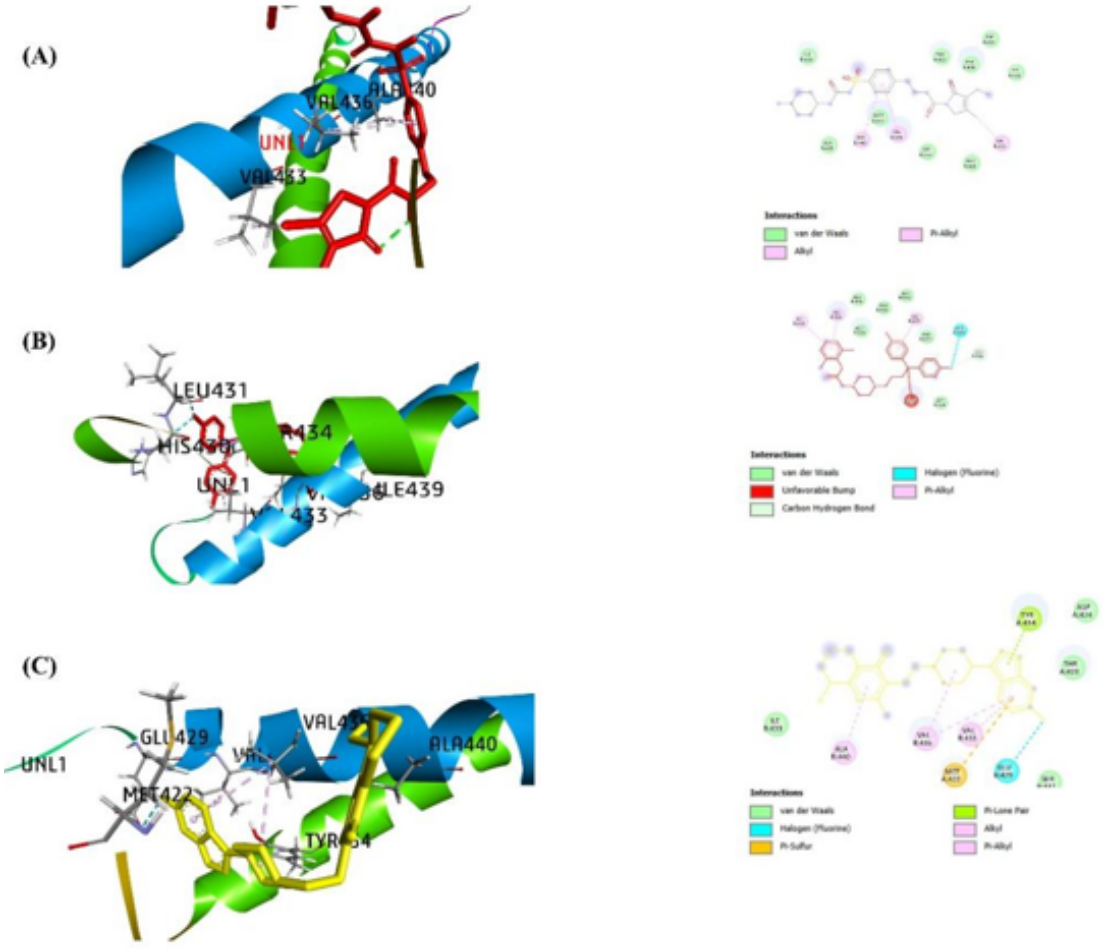


**Figure 3:** FDA-approved medication candidates that target BDNF using molecular docking analysis. Three-dimensional docking conformations of (A) Glimepiride, (B) Lidoflazine, and (C) Paliperidone within the BDNF binding pocket (PDB ID: 8OYD). Hydrogen bonds are represented by dashed lines, and hydrophobic interactions are shown as surface contacts. Binding energies calculated using AutoDock Vina indicate strong binding affinity, with Lidoflazine exhibiting the most favorable docking score.

## Molecular Dynamic Simulation

### Structural Stability Analysis (RMSD)

The backbone RMSD of the protein–ligand complexes was monitored over the 200 ns molecular dynamics simulation to evaluate their structural stability. All three

complexes exhibited an initial equilibration phase within the first 20-30 ns, after which the RMSD values stabilized within an acceptable range. The Glimepiride-protein complex demonstrated relatively stable behavior with minimal fluctuations throughout the simulation, indicating a consistent conformational state. In contrast, the Lidoflazine-protein complex showed comparatively higher RMSD deviations, particularly after ~120 ns, suggesting transient conformational rearrangements. The Paliperidone-protein complex maintained moderate fluctuations with an overall stable trajectory, although slight increases in RMSD were observed toward the later stages of the simulation. Importantly, none of the systems exhibited abrupt or sustained deviations, indicating the absence of major structural destabilization upon ligand binding (Figure 4A). Overall, the RMSD profiles suggest that all three protein–ligand complexes achieve and maintain structural stability under the simulated conditions, with Glimepiride showing the most consistent behavior.

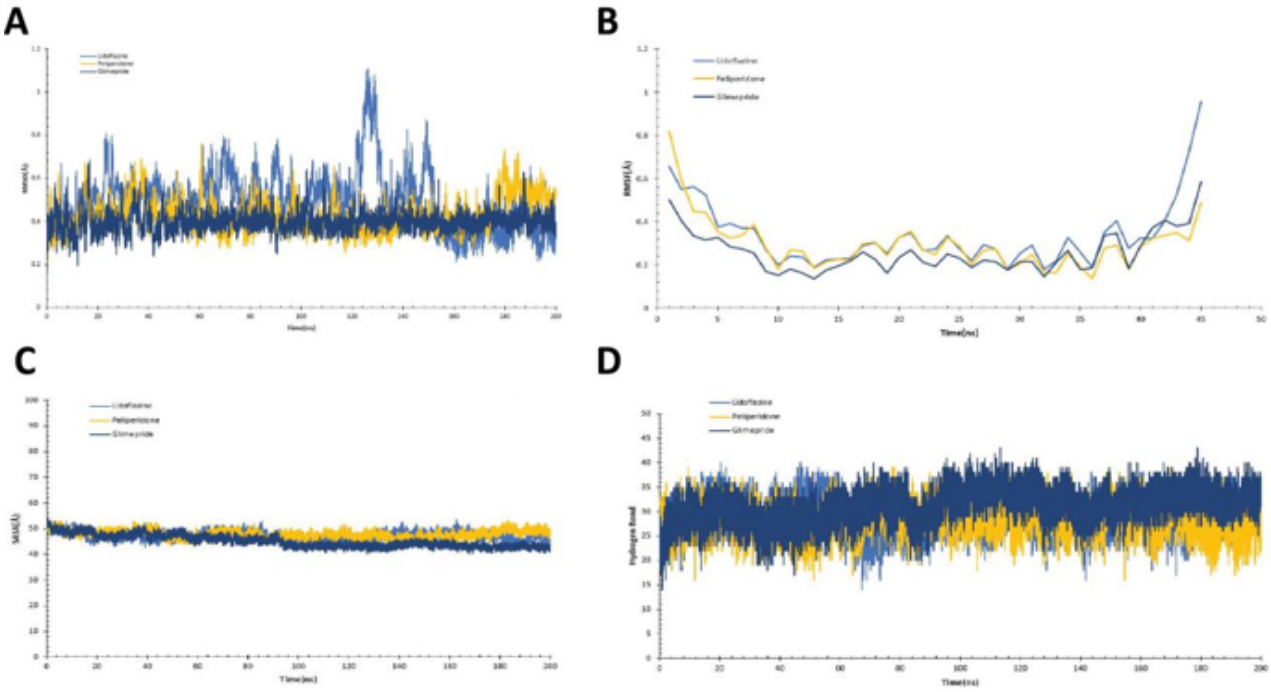


**Figure 4:** (A)Root mean square deviation (RMSD) of protein–ligand complexes over a 200 ns molecular dynamics simulation. The RMSD (Å) of the protein backbone is plotted against simulation time (ns) for complexes with Lidoflazine, Peliperidone, and Glimepiride. (B) Root mean square fluctuation (RMSF) profiles of protein residues in complex with Lidoflazine, Peliperidone, and Glimepiride during the molecular dynamics simulation. RMSF (Å) is plotted as a function of residue index, representing the flexibility of individual amino acid residues. (C) Solvent-accessible surface area (SASA) of protein–ligand complexes with Lidoflazine, Peliperidone, and Glimepiride over a 200 ns molecular dynamics simulation. SASA (Å²) is plotted as a function of simulation time (ns) to evaluate changes in protein surface exposure to the solvent. (D) Number of hydrogen bonds formed between the protein and ligands (Lidoflazine, Peliperidone, and Glimepiride) during the 200 ns molecular dynamics simulation. The number of hydrogen bonds is plotted as a function of simulation time (ns) to evaluate interaction stability.

## Residue Flexibility Assessment (RMSF)

To evaluate residue-level flexibility, the root mean square fluctuation (RMSF) was calculated for all protein–ligand complexes. The results indicate that the majority of residues exhibit relatively low fluctuation values, particularly within the core and binding pocket regions, suggesting limited structural flexibility upon ligand binding (Figure 4B). In contrast, higher fluctuations are observed in the terminal and loop regions, which is consistent with their inherently dynamic nature. Among the complexes, the Glimepiride-protein complex demonstrates comparatively lower

RMSF values across most residues, indicating a more stable and rigid protein conformation. The Paliperidone-protein complex shows moderate fluctuations, maintaining a generally stable profile. In comparison, the Lidoflazine-protein complex exhibits relatively higher fluctuations, particularly at the terminal regions, suggesting increased flexibility in these areas. Despite these differences, the binding site residues across all complexes remain relatively stable, indicating that ligand binding does not induce significant local destabilization.

### Solvent Accessible Surface Area (SASA) Analysis

SASA analysis was performed to evaluate changes in the solvent-accessible surface area of the protein during the 200 ns molecular dynamics simulation. The results indicate that all three protein–ligand complexes maintain relatively stable SASA values throughout the simulation, suggesting the absence of significant conformational expansion or structural collapse. Minor fluctuations are observed across the trajectories, which are typical of dynamic systems under physiological conditions. Among the complexes, the Lidoflazine-protein complex exhibits slightly lower SASA values compared to Glimepiride and Paliperidone, indicating a marginally more compact protein conformation. In contrast, the Paliperidone-protein complex shows relatively higher SASA values, suggesting a slightly greater solvent-exposed surface (Figure 4C). However, these differences are not substantial, and all complexes display comparable surface behaviour overall. The consistent SASA profiles across the simulation further support the structural stability of the protein–ligand complexes.

### Hydrogen Bond Analysis

Hydrogen bond analysis was performed to evaluate the stability and persistence of intermolecular interactions between the ligands and the protein throughout the 200 ns molecular dynamics simulation. The results indicate the continuous formation of hydrogen bonds in all three complexes, demonstrating stable ligand–protein interactions over the simulation period. Among the complexes, the Glimepiride-bound complex exhibits a comparatively higher number of hydrogen bonds with consistent fluctuations, indicating a more extensive hydrogen bonding network (Figure 4D). The Lidoflazine complex shows moderate hydrogen bond formation, while the Paliperidone complex maintains relatively lower hydrogen bond counts throughout the simulation. Despite these differences, all complexes display sustained hydrogen bonding interactions, suggesting that polar contacts play a significant role in maintaining the stability of the protein–ligand complexes.

## Discussion

Diabetic nephropathy is the major cause of last-stage renal dysfunction around the globe [25]. The primary potential causes of DN are chronic hyperglycemia and excessive blood pressure [26]. Recent discoveries suggest that several pathways are active during the progression of diabetes mellitus and that these pathways, separately or jointly, participate in the initiation and advancement of diabetic nephropathy. Unfortunately, treatment interventions targeting these pathways to control diabetic nephropathy are still unsuccessful [27,28] despite the indication that the number of people with diabetes and nephropathy is expanding year after year [25]. RNA-Seq is a promising method for transcriptome mapping that makes use of deep-sequencing technology [29]. RNA-Seq also allows a significantly more exact determination of transcript quantities and isoforms than other approaches. The purpose of this analysis was to demonstrate that the gene expression profile in diabetic nephropathy tissue differs from normal tissues and that the significantly regulated genes in diabetic nephropathy samples have functional roles with therapeutic properties. The gene expression analysis determines a total of 203 DEGs, including 147 upregulated and 56 downregulated genes. The rest of the genes were non-significant genes, The number of up--regulated genes was greater than the number of down- regulated genes, which corresponded to the original published report. The most significant overexpressed upregulated gene was ENSG00000198786, showing the highest expression, which is also shown in the Volcano plot of Log2 of Fold Change and -Log10 p-values. The other top significant genes which were shown in the plot were ENSG00000203865, ENSG000000198886, and ENSG00000189223. The DEGs were determined to be highly enriched in the oxytocin signaling pathway, thyroid hormone pathway, arrhythmogenic right ventricular cardiomyopathy, actin- binding, toll-like receptor binding, and neutrophil activation in the analysis in DAVID [30]. The expres-

sion levels of genes and their corresponding miRNAs could help to elucidate the pathophysiology of DN through targeted slicing. Among the hub genes, IRF1 shows the highest degree. IRF-1 was an up-regulated gene in diabetic nephropathy [31].

The overexpression of this gene induces the profibrotic marker expression, which results in the down-regulation of KIotho (inhibitor factor), thus resulting in renal fibrosis or acute diabetic nephropathy [32]. IRF1 is a positive regulator of the upregulated gene in response to high glucose levels [33]. IRF1 overexpression hindered cell cycle progression under normal glucose concentrations by downregulating cyclin D1/CDK4 [34,35]. In high glucose circumstances, IRF1 overexpression increased cyclin E/CDK2 expression and accelerated cell cycle progression. ACGT1 was another hub node, encoding of ACTG-1 Actin gamma 1 is a critical feature of the cytoskeleton [33,36]. AceView predicts that the ACTG-1 protein produced by this gene will have molecular activities (nucleotide-binding, ATP-binding) and will be found in many regions (cytoplasm, cytoskeleton, nucleus) [36]. According to reports, ACTG-1 is expressed at a very high level in DN and has been linked to a variety of disorders, including neoplasms and kidney disease [36,37] . Recent research has shown that the MDM2 gene plays a crucial role in DM prevention. Nuclear factor erythroid 2-related factor 2 (NRF2) is a potent inhibitor of the cellular antioxidant system that is suppressed by P53 and prevents DN. Given that MDM2 is a critical negative regulator of P53, it promotes NRF2 antioxidant signaling in diabetic nephropathy. According to current research, the level of expression of miR-205-5p is very high in DN patients and is also considered a non-invasive biomarker in DN. The characterization of abnormal pathways in DN patients may aid in the identification of the precise biological process and the discovery of more fascinating and potential molecular concepts with efficient predictive and therapeutic value. These findings give information on the pathophysiology of DN and help to create tailored treatments. Moreover, further research is required to study the molecular mechanisms underlying these malfunctioning pathways and DN acquisition.

All-atom molecular dynamics simulations lasting 200 ns were performed in order to confirm the stability and dynamic behaviour of the discovered BDNF–drug complexes. Beyond static docking predictions, MD simulation offers a time-resolved evaluation of protein–ligand interactions that enables assessment of conformational stability in conditions that are close to physiological. Throughout the entire simulation time, all three complexes exhibited fast equilibration and stationary plateaus in their RMSD values. What is more interesting is that the Lidoflazine-BDNF complex exhibited the smallest fluctuation in RMSD values, the smallest solvent-accessible surface area, lower residue flexibility in the binding site of the protein (RMSF), and the highest hydrogen bonding. These factors indicate a more compact and stable protein-ligand complex. These simulations confirm the potential of the drug lidoflazine as a modulator of BDNF and reinforce the accuracy of the docking prediction. Most importantly, the absence of significant changes in the protein structure during the simulations confirms that the binding of the drug does not induce any unfavorable changes in the protein structure. The MD simulations confirm the potential of the drug in treating diabetic nephropathy through its action on BDNF.

## Conclusion

This integrative approach comprehensively analyzed the transcriptomic changes in diabetic nephropathy (DN) using RNA-Seq, where 203 differentially expressed genes were identified, including those involved in mitochondrial dysfunction, oxidative stress, and metabolic disorders. Weighted Gene Co-expression Network Analysis (WGCNA) and Protein-Protein Interaction (PPI) mapping identified BDNF as a key hub gene, extensively regulated by multiple miRNAs, as well as other key hub genes, including IRF1, STAT1, ACTG1, UBC, and MDM2. Additionally, the miRNA/hub gene network, including hsa-miR-205-5p, revealed key post-transcriptional regulatory mechanisms involved in the development of diabetic nephropathy.

Virtual screening and molecular docking studies revealed that Glimepiride, Lidoflazine, and Paliperidone are potent BDNF modulators of high affinity. The simulations of molecular dynamics further validated their stability and persistent interactions. Overall, this study provides new insights into the molecular mechanisms of DN. It points out potential biomarkers and proposes new therapeutic ap-

proaches for the treatment of diabetic nephropathy. This study provides a foundation for future experimental validation of new therapeutic approaches for the treatment of diabetic nephropathy.

## References


1. Ala M (2023) Sestrin2 Signaling Pathway Regulates Podocyte Biology and Protects against Diabetic Nephropathy. J Diabetes Res. 2023: 1–15.

2. Baldoni PL, Chen Y, Hediyeh-zadeh S, et al. (2024) Dividing out quantification uncertainty allows efficient assessment of differential transcript expression with edgeR. Nucleic Acids Res. 52: e13.

3. Barutta F, Bellini S, Gruden G (2022) Mechanisms of podocyte injury and implications for diabetic nephropathy. Clin Sci. 136: 493–520.

4. Dong W, Zhang H, Zhao C, et al. (2021) Silencing of miR-150-5p Ameliorates Diabetic Nephropathy by Targeting SIRT1/p53/AMPK Pathway. Front Physiol. 12: 624989.

5. Fagundes R, Teixeira LK (2021) Cyclin E/CDK2: DNA Replication, Replication Stress and Genomic Instability. Front Cell Dev Biol. 9: 774845.

6. Gao Y, Li L, Amos CI, et al. (2021) Analysis of alternative polyadenylation from single-cell RNA-seq using scDaPars reveals cell subpopulations invisible to gene expression. Genome Res. 31: 1856–66.

7. Gao Y, Wang F, Wang R, et al. (2023) ESPRESSO: Robust discovery and quantification of transcript isoforms from error-prone long-read RNA-seq data. Sci Adv. 9: eabq5072.

8. Guo M, Dai Y, Jiang L, et al. (2022) Bioinformatics Analysis of the Mechanisms of Diabetic Nephropathy via Novel Biomarkers and Competing Endogenous RNA Network. Front Endocrinol. 13: 934022.

9. Guo M, Gao J, Jiang L, et al. (2023) Astragalus Polysaccharide Ameliorates Renal Inflammatory Responses in a Diabetic Nephropathy by Suppressing the TLR4/NF-κB Pathway. Drug Des Devel Ther. 17: 2107–18.

10. Han D, Zhu S, Li X, et al. (2022) The NF-κB/miR-488/ERBB2 axis modulates pancreatic cancer cell malignancy and tumor growth through cell cycle signaling. Cancer Biol Ther. 23: 294–309.

11. Han Y-P, Liu L-J, Yan J-L, et al. (2023) Autophagy and its therapeutic potential in diabetic nephropathy. Front Endocrinol. 14: 1139444.

12. Hu Y, Liu S, Liu W, et al. (2021) Bioinformatics analysis of genes related to iron death in diabetic nephropathy through network and pathway levels based approaches. PLOS ONE, 16: e0259436.

13. Klein AM, Biderman L, Tong D, et al. (2021) MDM2, MDMX, and p73 regulate cell-cycle progression in the absence of wild-type p53. Proc Natl Acad Sci. 118: e2102420118.

14. Klein AM, De Queiroz RM, Venkatesh D, et al. (2021) The roles and regulation of MDM2 and MDMX: it is not just about p53. Genes Dev. 35: 575–601.

15. Li B, Zhao X, Xie W, et al. (2023) Integrative analyses of biomarkers and pathways for diabetic nephropathy. Front Genet. 14: 1128136.

16. Li X, Gao L, Li X, et al. (2024) Autophagy, Pyroptosis and Ferroptosis are Rising Stars in the Pathogenesis of Diabetic Nephropathy. Diabetes Metab Syndr Obes. 17: 1289–99.

17. Liu J, Wang J, Fu W, et al. (2021) MiR-195-5p and miR-205-5p in extracellular vesicles isolated from diabetic foot ulcer wound fluid decrease angiogenesis by inhibiting VEGFA expression. Aging, 13: 19805–21.

18. Healthcare Engineering JO (2023) Retracted: Construction and Bioinformatics Analysis of the miRNA-mRNA Regulatory Network in Diabetic Nephropathy. J Healthc Eng. 2023: 9858642.

19. Liu J, Liu Z, Sun W, et al. (2023) Role of sex hormones in diabetic nephropathy. Front Endocrinol. 14: 1135530.

20. Lu K, Wang L, Fu Y, et al. (2022) Bioinformatics analysis identifies immune-related gene signatures and subtypes in diabetic nephropathy. Front Endocrinol. 13: 1048139.

21. Khalid HR, Aamir M, Tabassum S, et al. (2022) Integrated System Pharmacology Approaches to Elucidate Multi--Target Mechanism of Solanum surattense against Hepatocellular Carcinoma. Molecules. 27: 6220.

22. Tabassum S, Khalid HR, Haq WU, et al. (2022) Implementation of System Pharmacology and Molecular Docking Approaches to Explore Active Compounds and Mechanism of Ocimum Sanctum against Tuberculosis. Processes, 10: 298.

23. Wu N, Zhang R, Peng X, et al. (2024) Elucidation of protein–ligand interactions by multiple trajectory analysis methods. Phys Chem Chem Phys. 26: 6903–15.

24. Li M (2024) Molecular Dynamics Simulations: A Systematic Review of Techniques and Applications in Biochemistry. Comput Mol Biol. Epub ahead of print.

25. Zhao H, Yang C-E, Liu T, et al. (2023) The roles of gut microbiota and its metabolites in diabetic nephropathy. Front Microbiol. 14: 1207132.

26. Yang J, Liu Z (2022) Mechanistic Pathogenesis of Endothelial Dysfunction in Diabetic Nephropathy and Retinopathy. Front Endocrinol. 13: 816400.

27. Maiti AK (2021) Development of Biomarkers and Molecular Therapy Based on Inflammatory Genes in Diabetic Nephropathy. Int J Mol Sci. 22: 9985.

28. Zhou H, Ni W-J, Meng X-M, et al. (2021) MicroRNAs as Regulators of Immune and Inflammatory Responses: Potential Therapeutic Targets in Diabetic Nephropathy. Front Cell Dev Biol. 8: 618536.

29. Pardo-Palacios FJ, Wang D, Reese F, et al. (2024) Systematic assessment of long-read RNA-seq methods for transcript identification and quantification. Nat Methods. 21: 1349–63.

30. Zhu H, Chen Y, Gong W, et al. (2022) Shared and specific biological signalling pathways for diabetic retinopathy, peripheral neuropathy and nephropathy by high--throughput sequencing analysis. Diab Vasc Dis Res. 19: 14791641221122918.

31. Wu L, Cheng Q, Wen Z, et al. (2021) IRF1 as a potential biomarker in Mycobacterium tuberculosis infection. J Cell Mol Med. 25: 7270–9.

32. Miao J, Huang J, Luo C, et al. (2021) Klotho retards renal fibrosis through targeting mitochondrial dysfunction and cellular senescence in renal tubular cells. Physiol Rep; 9.

33. Mohandes S, Doke T, Hu H, et al. (2023) Molecular pathways that drive diabetic kidney disease. J Clin Invest. 133: e165654.

34. Ni W, Guan X, Zeng J, et al. (2022) Berberine regulates mesangial cell proliferation and cell cycle to attenuate diabetic nephropathy through the PI3K/Akt/AS160/GLUT1 signalling pathway. J Cell Mol Med. 26: 1144–55.

35. Zhang W, Liu Y, Jang H, et al. (2024) CDK2 and CDK4: Cell Cycle Functions Evolve Distinct, Catalysis-Competent Conformations, Offering Drug Targets. JACS Au. 4: 1911–27.

36. Xiao L, Peng H, Yan M, et al. (2021) Silencing ACTG1 Expression Induces Prostate Cancer Epithelial Mesenchymal Transition Through MAPK/ERK Signaling Pathway. DNA Cell Biol. 40: 1445–55.

37. Liu S, Wu W, Liao J, et al. (2022) MicroRNA-21: A Critical Pathogenic Factor of Diabetic Nephropathy. Front Endocrinol. 13: 895010.